Two-Dimensional Electron Gases at $LaAlO_3/SrTiO_3$ Interfaces: Orbital Symmetry and Hierarchy Engineered by Crystal Orientation

D. Pesquera,[1] M. Scigaj,[1,2] P. Gargiani,[3] A. Barla,[4] J. Herrero-Martín,[3] E. Pellegrin,[3] S. M. Valvidares,[3] J. Gázquez,[1] M. Varela,[5,6] N. Dix,[1] J. Fontcuberta,[1] F. Sánchez,[1] and G. Herranz[1,*]

[1]*Institut de Ciència de Materials de Barcelona (ICMAB-CSIC), Campus de la UAB, Bellaterra E-08193, Catalonia, Spain*
[2]*Departamento de Física, Universitat Autònoma de Barcelona, E-08193 Bellaterra, Barcelona, Catalonia, Spain*
[3]*ALBA Synchrotron Light Source, Carretera BP 1413 km 3.3, E-08290 Cerdanyola del Vallès, Barcelona, Spain*
[4]*Istituto di Struttura della Materia, ISM CNR, Area Science Park Basovizza (Ts), Trieste I-34149, Italy*
[5]*Departamento Física Aplicada III, Universidad Complutense de Madrid, Madrid, 28040 Spain*
[6]*Materials Science and Technology Division, Oak Ridge National Laboratory, Oak Ridge, Tennessee 37831, USA*

(Received 9 May 2014; revised manuscript received 24 July 2014; published 7 October 2014)

Recent findings show the emergence of two-dimensional electron gases (2DEGs) at $LaAlO_3/SrTiO_3$ interfaces along different orientations; yet details on band reconstructions have remained so far unknown. Via x-ray linear dichroism spectroscopy, we demonstrate that crystal symmetry imposes distinctive 2DEG orbital hierarchies on (001)-and (110)-oriented quantum wells, allowing selective occupancy of states of different symmetry. Such orientational tuning expands the possibilities for electronic engineering of 2DEGs and opens up enticing opportunities to understand the link between orbital symmetry and complex correlated states at $LaAlO_3/SrTiO_3$ quantum wells.

DOI: 10.1103/PhysRevLett.113.156802 PACS numbers: 73.20.At, 73.21.Fg

The electronic structure of solids is deeply modified whenever the dimensionality of the system is reduced. One particular case occurs when the electron motion is confined within a plane in quantum well structures. For instance, in the realm of III-V or II-VI semiconductors, selecting a particular quantization direction for the quantum well growth is fundamental to achieve optimum efficiency for optoelectronic applications [1–3]. This is attained by a judicious selection of the crystal orientation that confines the electron motion, so that the effective masses or the internal polarization fields can be largely modulated to values that optimize the device performance.

Beyond these more conventional systems, the recent discovery of quantum well structures based on the *d*-band $SrTiO_3$ oxide semiconductor has broken new ground [4–11]. The basic reasons are (i) the extremely confined character of the oxide quantum wells (of the order of a few nanometers) and (ii) a sheet carrier density above one order of magnitude higher than in conventional semiconductors. In addition, the much narrower bandwidth of *d*-derived electronic levels of transition metals—as compared to the wide *s* or *p* bands—promotes the emergence of complex electronically correlated states not present in the traditional semiconductors. Epitomizing this complexity, both magnetism and superconductivity have been reported to emerge at the $LaAlO_3/SrTiO_3$ interface [12–15], which is the most intensively investigated system of this kind. The possibility of applying electrostatic gate voltages to these extremely narrow quantum wells [16–18] provides a unique opportunity to explore fundamental questions in the field of quantum fluids [19,20]. One of these aspects is related to the possible multiband character of superconductivity at the $SrTiO_3$-quantum wells and its connexion with the detailed orbital structure of the t_{2g} states [21,22]. The microscopic nature of the interface magnetism has also been linked to the orbital energy hierarchy of t_{2g} and e_g levels [23,24] and even spectroscopic investigations emphasize the specific role of d_{xy} states regarding the emergence of magnetism [25].

While the vast majority of these studies have been carried out on (001)-oriented oxide quantum wells, recent works have demonstrated that two-dimensional electron gases (2DEGs) can also be generated along other crystal orientations [26–28], opening up novel perspectives in the physical understanding of low-dimensional complex phases. Yet, the mechanisms driving the emergence of 2DEGs confined along these unconventional orientations are far from being understood. Recently, a common origin has been proposed for 2DEGs at (001) and (110) interfaces, i.e., relaying on the polar discontinuity to trigger a charge transfer across the interface [27]. This raises the question whether the 2DEGs along these interfaces are really different. In other words, do they share a common orbital hierarchy or, on the contrary, the electronic band structure is reconstructed when the quantum well orientation is changed. Our work settles this question altogether because (i) we show conclusively that the (110) interface is free from any faceting that could generate a (001) 2DEG, and, more important, (ii) our work unambiguously demonstrates that the electronic structure of the 2DEG along [110] is intrinsically different from the one along [001].

Our conclusion is based on x-ray linear dichroism (XLD) experiments at the Ti-L_2 and L_3 edges. From the analysis of the XLD spectra, a picture emerges in which the degeneracy within the t_{2g} and e_g subbands is broken. Such kind of lifted degeneracy has been observed previously in (001)-oriented $LaAlO_3/SrTiO_3$ [29] or $SrTiO_3$ surfaces [30,31], and has been attributed to the combined effects of low-temperature tetragonal distortions, spin-orbit coupling, and quantum well confinement [30]. Here, however, we show that orbital symmetry is a key ingredient to further engineer the 2DEG band structure of $LaAlO_3/SrTiO_3$ quantum wells, expanding vigorously the possibilities to investigate the link between orbital symmetry and complex electronic phases at these interfaces [22,25]. Briefly, for (001)-oriented 2DEGs, we find that d_{xy} and d_{x2-y2} orbitals are the lowest energy levels of t_{2g} and e_g symmetry, respectively, confirming theoretical predictions as well as previous spectroscopic studies [29,32]. Remarkably, however, we show that (110)-oriented 2DEGs exhibit a distinct electronic structure, where the bottommost levels have instead a d_{xz}/d_{yz} and d_{3z2-r2} character.

The samples covered by this study were grown by pulsed laser deposition assisted with *in situ* reflection high-energy electron diffraction (RHEED) on (001)- and (110)-oriented $SrTiO_3$ single crystals. $LaAlO_3$ films of different thicknesses t were deposited, with $t = 0$ and 8 monolayers (MLs) for (001) and $t = 0$, 2, and 9 MLs for (110), respectively, -1 ML ≈ 3.79 Å for (001) and 1 ML ≈ 2.68 Å for (110). Note that the surface of bare $SrTiO_3$ crystals was included in the analysis, providing access to the initial surface electronic structure prior to deposition of the $LaAlO_3$ layers. The $SrTiO_3$ substrates oriented along [001] were not chemically treated before film deposition. In these conditions, the surface has mostly TiO_2 termination, with just a residual presence of minority SrO termination [33,34]. $SrTiO_3(110)$ substrates were thermally treated to obtain an atomically flat surface as observed by atomic force microscopy [26,28]. We stress that postgrowth *in situ* annealing was part of the thin film preparation process to promote the removal of residual oxygen vacancies during the growth [35]. Additionally, low temperature magnetotransport backs up the two-dimensional character of these quantum wells [28].

We carried out atomic-scale structural characterization to assess the quality of the interfaces. For that purpose, we performed high angle annular dark field (HAADF) imaging in a NION UltraSTEM200 (operated at 200 kV) and in a FEI Titan (60–300 kV) scanning transmission electron microscope (STEM), equipped with a Nion and a CEOS probe-aberration corrector, respectively. Figures 1(a) and 1(b) show the cross sectional HAADF-STEM images of (001)-and (110)-oriented $LaAlO_3/SrTiO_3$ interfaces along the [100] and [001] zone axes, respectively. From the HAADF imaging, the epitaxial $LaAlO_3$ layers are visible, being continuous over long lateral lengths (of the order of one micron). Under HAADF conditions the atomic-columns intensity scales approximately with the atomic number (Z) squared [36]. In this situation, the brightest spots in Fig. 1 represent the heaviest atomic columns, La, followed by Sr, Ti, and finally, by Al, which gives the weakest contrast. In the particular case of the (110) interface, the (110) ionic stacking across the interface can be readily appreciated, see Fig. 1(b). HAADF-STEM images show that the (001)-and (110)-oriented interfaces are atomically flat. Any reconstructed surfaces with local {100} microfacets are ruled out for the (110) interfaces. The two interfaces are quite different from the structural point of view and the electron orbital configuration should, correspondingly, exhibit distinctive features. In the following, we discuss how we determined the orbital hierarchy for the two crystal orientations.

For that purpose, experiments were done at the BOREAS beam line of the ALBA synchrotron radiation source to carry out room-temperature x-ray absorption spectroscopy (XAS) at the Ti-$L_{2,3}$ edges in total electron yield (TEY) mode. The main peaks featured in the XAS spectra result from transitions from Ti-$2p_{1/2}$ (L_2) and Ti-$2p_{3/2}$ (L_3) core levels to unoccupied Ti $3d$ states and have a contribution from t_{2g} (d_{xz}, d_{yz}, and d_{xy}) and e_g (d_{3z2-r2} and d_{x2-y2}) levels. Figure 2 shows a schematic description of the relationship between the photon beam linear polarization and the orbital symmetries. In all cases, the linear polarization vector E_a (red) was always kept in plane, i.e., $E_a \parallel [100]$ for (001) and

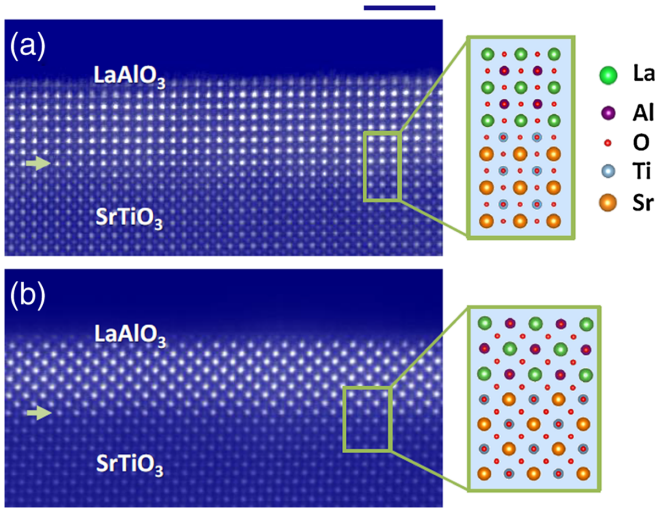

FIG. 1 (color online). (a) and (b), scanning transmission electron microscopy (STEM) high-angle annular dark field (HAADF) images of $LaAlO_3$(8 MLs)/$SrTiO_3$(001) and a $LaAlO_3$(9 MLs)/$SrTiO_3$(110) samples, respectively. The (a) and (b) images were acquired in a Nion UltraSTEM200 and in a FEI Titan (60–300 kV), respectively, and have been Fourier filtered to reduce background noise. The zone axes are along [100] and [001], respectively. Green arrows point to the $LaAlO_3/SrTiO_3$ interface, easily distinguished due to the different intensities between individual La and Sr atomic columns. The scale bar corresponds to a length of 2 nm. The panels on the right hand side show the schematic structure of both interfaces.

$E_a \parallel [001]$ for (110) samples, respectively. Instead, polarization E_b (blue) was either in plane (normal incidence) or out of plane (grazing incidence). The orientation of E_b with respect to the crystal axes is given in Figs. 2(a)–2(d) for each case. X-ray induced electronic transitions to the d orbitals have an intensity that depends on the orbital symmetry of the available d final states, the interaction being strongest when light polarization is along the direction of the orbital lobes [37]. The sketch in the inset of Fig. 2 graphically depicts the different possibilities of electric field projection onto the orbital lobes. The TEY intensities I_a and I_b were recorded for the two orthogonal E_a and E_b polarizations, and the XLD signal was defined as the difference $\mathrm{XLD} = (I_a - I_b)$.

XLD spectra were recorded with x-ray beams at normal [Figs. 2(a)–2(b)] and at grazing incidence [Figs. 2(c)–(d)]. Experiments at normal incidence were crucial to prove unambiguously that the interfaces had different crystal orientations. Conversely, XLD spectra measured at grazing incidence were indispensable to obtain the orbital hierarchy. The reason is that the shape of the XLD spectra is reversed when the symmetry axis of the orbitals with lower energy are projected either along the in-plane or out-of-plane directions, as schematically shown in Figs. 2(e)–2(f). At grazing incidence [Figs. 2(c)–2(d)], the orbitals that couple most intensely with the in-plane vector E_a are d_{xy}/d_{x2-y2} for the (001) interface and $d_{xz}/d_{yz}/d_{3z2-r2}$ for (110); those that couple strongly with the out-of-plane vector E_b are $d_{xz}/d_{yz}/d_{3z2-r2}$ and d_{xy}/d_{x2-y2} for (001) and (110), respectively. Thus, the orbitals involved in the electron transitions having a larger scattering cross section with light of a given polarization have complementary symmetries when we switch between the (001) and (110) orientations. As a result, and anticipating the results discussed below, the mere observation of the same sign for XLD spectra measured at (001) and (110) interfaces unequivocally implies that the orbital hierarchy is reversed when the 2DEG confinement is switched between [001] and [110] orientations.

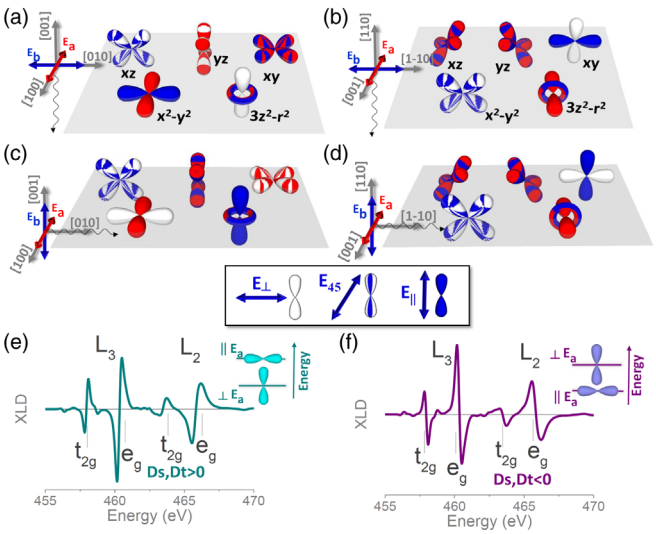

FIG. 2 (color online). Schematics of the interaction of linearly polarized light with d orbitals for normal incidence of x rays on (001)-oriented samples (a) and (110)-oriented samples (b); same schematics for the case of grazing incidence on (001) samples (c) and (110) samples (d). The color shading code is shown in the box. Simulations of XLD signal $(I_a - I_b)$ for Ti^{4+} in tetragonal crystal field with positive (e) and negative (f) distortion parameters. The corresponding orbital hierarchy is shown, as related to the relative orientation of light polarization and orbitals.

We first discuss experiments done at normal incidence. Due to the inherent fourfold in-plane symmetry for (001) samples, light should be absorbed equally for both photon polarizations. This is confirmed by the negligible XLD of the (001)-$LaAlO_3/SrTiO_3$ interface ($t = 8$ MLs). In contrast, the anisotropic character of (110) interfaces imprints a distinctive nonzero XLD, as observed in the spectrum of the (110) interface ($t = 9$ MLs), see Fig. 3(b). In order to unveil the details of the reconstructed electronic structures, XAS spectra were measured also at grazing incidence (60° away from the normal) that, in turn, allowed us quantifying the splitting between the t_{2g} and e_g substates. Since $LaAlO_3/SrTiO_3$ interfaces have a threshold $LaAlO_3$

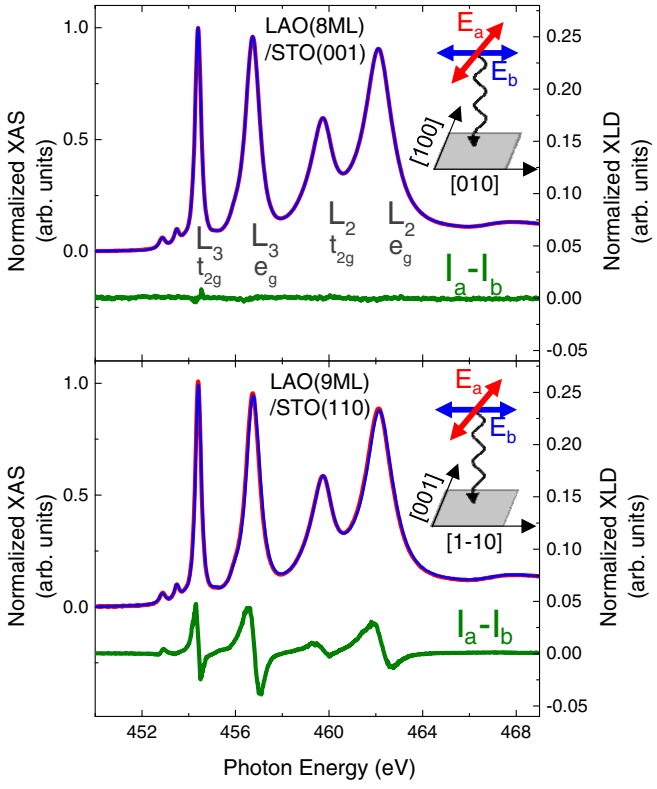

FIG. 3 (color online). (a) Normalized XAS spectra of sample $LaAlO_3$(8 MLs)/$SrTiO_3$(001) measured at normal incidence are shown. XAS curves are plotted for $E_a \parallel [100]$ (I_a) and $E_b \parallel [010]$ (I_b) polarizations. The XLD spectra $(I_a - I_b)$ are also shown. (b) Normalized XAS and XLD spectra of sample $LaAlO_3$(9 MLs)/$SrTiO_3$(110). Here, the polarizations are $E_a \parallel [001]$ and $E_b \parallel$ [0–10].

thickness (t_c) below which no conduction is observed ($t_c = 4$ MLs for [001] [4], $t_c = 7$ MLs for [110] [26]), we included the spectra of bare $SrTiO_3$ surfaces as well as subcritical interfaces that do no host any 2DEG. Previously, XLD of bare $SrTiO_3$ surfaces and subcritical interfaces were reported for the [001] orientation; here, we enlarge the same analysis for their counterparts along [110]. The XAS and XLD spectra recorded at grazing incidence on bare $SrTiO_3$ are shown in Figs. 4(a)–4(d). The XLD spectra—shifted vertically for the sake of clarity—demonstrate that the degeneracy of the t_{2g} and e_g states is already broken in the uncapped surfaces. More specifically, the sign of the XLD implies that the lower energy states have d_{xz}/d_{yz} and d_{3z2-r2} character for (001) interfaces, while they have d_{xy} and d_{x2-y2} character for (110) interfaces. The observed degeneracy breaking at $SrTiO_3$ surfaces mimics the behavior observed for (001)- and (110)-oriented manganites [38], in which the symmetry rupture at free surfaces is responsible for the orbital reconstruction.

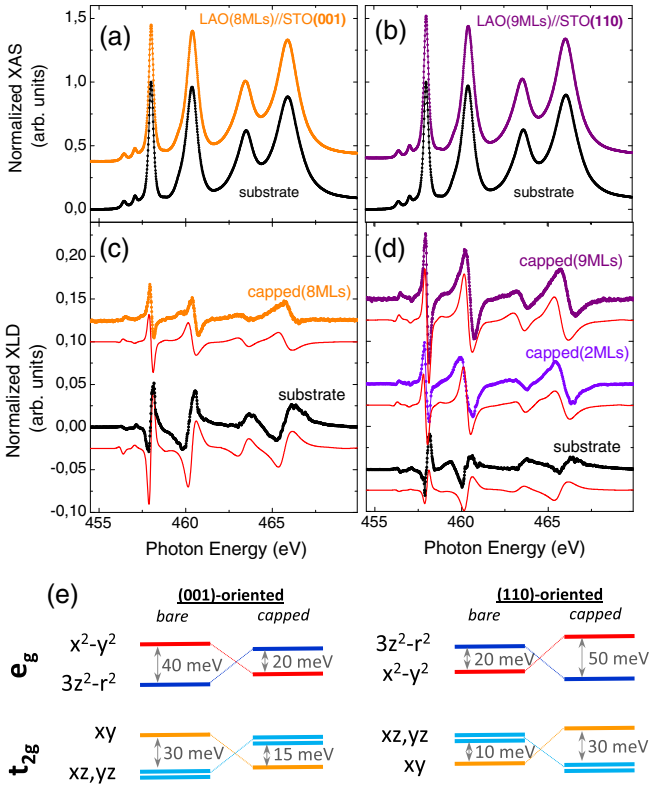

FIG. 4 (color online). Normalized XAS spectra measured at grazing incidence are plotted for bare $SrTiO_3$ surfaces as well as $LaAlO_3/SrTiO_3$ interfaces for orientation along (a) [001] and (b) [110]. The $LaAlO_3$ thickness is 8 MLs for (001) and 9 MLs for (110) interfaces. The corresponding XLD spectra are shown for (001)- and (110)-oriented samples in (c) and (d), respectively. Note that (d) also includes the XLD for $LaAlO_3/SrTiO_3$ with thickness 2 MLs. Red lines, corresponding to XLD simulations using CTM4XAS, are shifted for clarity. Finally, the energy splittings for (001)- and (110)-oriented samples are sketched in (e).

We discuss now the XLD spectra [Figs. 4(c) and 4(d)] acquired from samples in which the $SrTiO_3$ surface was capped by $LaAlO_3$. We have found that supracritical interfaces—hosting a 2DEG—with $LaAlO_3$ thickness $t =$ 8 MLs for [001] and $t = 9$ MLs for [110]—have an electronic structure that is reconstructed from that of bare surfaces. More specifically, d_{xy} and d_{x2-y2} states were found to be lower in energy for the (001) interface, whereas the lowest energy t_{2g} and e_g orbitals had mostly d_{xz}/d_{yz} and d_{3z2-r2} character for confinement along [110]. The orbital hierarchy observed in our experiments for the (110) interface is consistent with that reported recently for 2DEGs generated at the bare (110)-oriented $SrTiO_3$ surface [39]. We thus observed that the degeneracy within the t_{2g} and e_g subbands is broken in opposite directions for bare and capped surfaces. Similarly to (001)-oriented interfaces [29], such orbital hierarchy inversion with respect to bare surfaces is already observed at (110)-oriented subcritical $LaAlO_3$ thickness [$t = 2$ MLs, see XLD spectra in Fig. 4(d)], i.e., at interfaces that do not show any macroscopic conductance.

For a quantitative description of the reconstructed bands, we performed atomic model calculations using the CTM4XAS software [40] using typical crystal field and charge transfer parameters for Ti^{4+} in octahedral coordination to fit the experimental XLD curves [41]. The simulated spectra are included in Figs. 4(c)–4(d) (red lines). Figure 4(e) summarizes all the information extracted from CTM4XAS simulations. We restrict the discussion to supracritical interfaces hosting the high-mobility 2DEG. Our first conclusion is that in (001)-oriented interfaces d_{xy} orbitals are lower than d_{xz}/d_{yz} levels by ~15 meV, whereas d_{x2-y2} states are shifted down with respect to d_{3z2-r2} by about 20 meV. Secondly, we conclude that the orbital energy hierarchy of (110)-oriented 2DEGs is reconstructed in an inverted way; i.e., d_{xz}/d_{yz} and d_{3z2-r2} states are lower than d_{xy} and d_{x2-y2} by 30 meV and 50 meV, respectively. We note that variations in the sheet carrier density may cause a nonrigid evolution of the band structure in $LaAlO_3/SrTiO_3$ interfaces [42] that could have eventually an influence on the energy splittings within the e_g and t_{2g} subbands. Bearing this in mind, and for the sake of completeness, we specify explicitly the values of the sheet carrier density of our samples, i.e., $n_{\mathrm{sheet}} \approx 2.5 \times 10^{13}$ cm^{-2} and $n_{\mathrm{sheet}} \approx 8 \times 10^{13}$ cm^{-2} for (001) and (110), respectively. Although an eventual role of the sheet carrier density would explain why the splittings for the (001) $LaAlO_3/SrTiO_3$ interface extracted from our analysis are smaller than those reported by M. Salluzzo *et al.* [29], we emphasize that the inferred electronic state hierarchy is the same in both cases. We can thus conclude that the 2DEG along the (110) orientation has an unambiguously genuine band structure, completely different from that of the (001) 2DEG, being the hierarchy of states with different symmetry totally reversed.

In summary, our results establish crystal symmetry as an extra degree of freedom to realize different 2DEG band reconstructions at the $LaAlO_3/SrTiO_3$ interface, thus

allowing a selective occupancy of states of different symmetry. These results open up new opportunities for 2DEG band engineering and are crucial to extend our current understanding of the link between orbital symmetry and complex correlated states, such as magnetism or superconductivity. One could, for instance, anticipate a different spatial extent of 2DEGs due to different bandwidths of electron states upon reversal of the orbital hierarchy. Indeed, our preliminary results demonstrate that 2DEGs confined along (110) have a significant broader extension than along (001), implying a larger anisotropy of the two-dimensional superconductive state for the latter [28]. Beyond that, we further envision electrostatic gating as a privileged pathway to probe the properties of these quantum wells. Recently, a connection has been established between d_{xy} orbitals and magnetism [25]. This issue can be further investigated in a controlled experiment, during which electrostatic fields can be adjusted to fill selectively—at low doping levels—the d_{xy} or d_{xz}/d_{yz} states in (001) or (110) interfaces, respectively, while the magnetism is probed. By the same token, selective orbital occupancy combined with electrostatic gating would extend our present knowledge on intra- and interband pairing mechanisms of 2D superconductivity [21] as well as on the observed universal Lifshitz transition, by which a switch from one- to two-carrier transport takes place at a universal charge carrier density [22]. These, and other fascinating experiments, are possible by the crystal symmetry reconstruction of 2DEGs at the $LaAlO_3/SrTiO_3$ interfaces.

This work was supported by the Spanish Government through MAT2011-29269-C03, and NANOSELECT CSD2007-00041 projects and the Generalitat de Catalunya (2009 SGR 00376 project). J. G. acknowledges the Ramon y Cajal program (RYC-2012-11709). These experiments were performed at the Boreas beam line of the Synchrotron Light Facility ALBA with the collaboration of ALBA staff. Microscopy work was conducted in the STEM Group of the Oak Ridge National Laboratory (ORNL), and in the Laboratorio de Microscopías Avanzadas at the Instituto de Nanociencia de Aragón—Universidad de Zaragoza. Research at ORNL supported by the U.S. Department of Energy (DOE), Basic Energy Sciences (BES), Materials Sciences and Engineering Division (MV). Research at UCM supported by the ERC Starting Investigator Award STEMOX 739239.

*gherranz@icmab.cat

[1] S.-H. Park, J. Appl. Phys. **91**, 9904 (2002).
[2] M. Feneberg and K. Thonke, J. Phys. Condens. Matter **19**, 403201 (2007).
[3] S.-H. Park and D. Ahn, Opt. Quantum Electron. **38**, 935 (2006).
[4] A. Ohtomo and H. Y. Hwang, Nature (London) **427**, 423 (2004).
[5] A. Ohtomo, D. A. Muller, J. L. Grazul, and H. Y. Hwang, Nature (London) **419**, 378 (2002).
[6] H. W. Jang *et al.*, Science **331**, 886 (2011).
[7] J. Biscaras, N. Bergeal, A. Kushwaha, T. Wolf, A. Rastogi, R. C. Budhani, and J. Lesueur, Nat. Commun. **1**, 89 (2010).
[8] Y. Hotta, T. Susaki, and H. Y. Hwang, Phys. Rev. Lett. **99**, 236805 (2007).
[9] P. Perna *et al.*, Appl. Phys. Lett. **97**, 152111 (2010).
[10] P. Moetakef, J. Zhang, A. Kozhanov, B. Jalan, R. Seshadri, S. J. Allen, and S. Stemmer, Appl. Phys. Lett. **98**, 112110 (2011).
[11] Y. Z. Chen *et al.*, Nat. Commun. **4**, 1371 (2013).
[12] Lu Li, C. Richter, J. Mannhart, and R. C. Ashoori, Nat. Phys. **7**, 762 (2011).
[13] Ariando *et al.*, Nat. Commun. **2**, 188 (2011).
[14] J. A. Bert, B. Kalisky, C. Bell, M. Kim, Y. Hikita, H. Y. Hwang, and K. A. Moler, Nat. Phys. **7**, 767 (2011).
[15] B. Kalisky, J. A. Bert, B. B. Klopfer, C. Bell, H. K. Sato, M. Hosoda, Y. Hikita, H. Y. Hwang, and K. A. Moler, Nat. Commun. **3**, 922 (2012).
[16] A. D. Caviglia, S. Gariglio, N. Reyren, D. Jaccard, T. Schneider, M. Gabay, S. Thiel, G. Hammerl, J. Mannhart, and J.-M. Triscone, Nature (London) **456**, 624 (2008).
[17] N. Reyren *et al.*, Science **317**, 1196 (2007).
[18] C. Bell, S. Harashima, Y. Kozuka, M. Kim, B. G. Kim, Y. Hikita, and H. Y. Hwang, Phys. Rev. Lett. **103**, 226802 (2009).
[19] S. Caprara, J. Biscaras, N. Bergeal, D. Bucheli, S. Hurand, C. Feuillet-Palma, A. Rastogi, R. C. Budhani, J. Lesueur, and M. Grilli, Phys. Rev. B **88**, 020504(R) (2013).
[20] J. Biscaras, N. Bergeal, S. Hurand, C. Feuillet-Palma, A. Rastogi, R. C. Budhani, M. Grilli, S. Caprara, and J. Lesueur, Nat. Mater. **12**, 542 (2013).
[21] R. M. Fernandes, J. T. Haraldsen, P. Wolfle, and A. V. Balatsky, Phys. Rev. B **87**, 014510 (2013).
[22] A. Joshua, S. Pecker, J. Ruhman, E. Altman, and S. Ilani, Nat. Commun. **3**, 1129 (2012).
[23] N. Pavlenko, T. Kopp, E. Y. Tsymbal, G. A. Sawatzky, and J. Mannhart, Phys. Rev. B **85**, 020407(R) (2012).
[24] N. Pavlenko, T. Kopp, and J. Mannhart, Phys. Rev. B **88**, 201104(R) (2013).
[25] J.-S. Lee, Y. W. Xie, H. K. Sato, C. Bell, Y. Hikita, H. Y. Hwang, and C.-C. Kao, Nat. Mater. **12**, 703 (2013).
[26] G. Herranz, F. Sánchez, N. Dix, M. Scigaj, and J. Fontcuberta, Sci. Rep. **2**, 758 (2012).
[27] A. Annadi *et al.*, Nat. Commun. **4**, 1838 (2013).
[28] G. Herranz, N. Bergeal, J. Lesueur, J. Gazquez, M. Scigaj, N. Dix, F. Sanchez, and J. Fontcuberta. arXiv:1305.2411.
[29] M. Salluzzo *et al.*, Phys. Rev. Lett. **102**, 166804 (2009).
[30] A. F. Santander-Syro *et al.*, Nature (London) **469**, 189 (2011).
[31] S. M. Valvidares, M. Huijben, P. Yu, R. Ramesh, and J. B. Kortright, Phys. Rev. B **82**, 235410 (2010).
[32] P. Delugas, A. Filippetti, V. Fiorentini, D. I. Bilc, D. Fontaine, and P. Ghosez, Phys. Rev. Lett. **106**, 166807 (2011).
[33] F. Sánchez, C. Ocal, and J. Fontcuberta, Chem. Soc. Rev. **43**, 2272 (2014).
[34] M. Foerster, R. Bachelet, V. Laukhin, J. Fontcuberta, G. Herranz, and F. Sánchez, Appl. Phys. Lett. **100**, 231607 (2012).

[35] G. Herranz *et al.*, Phys. Rev. Lett. **98**, 216803 (2007).

[36] P. D. Nellist and S. J. Pennycook, Ultramicroscopy **78**, 111 (1999).

[37] J. Stöhr, J. Electron Spectrosc. Relat. Phenom. **75**, 253 (1995).

[38] D. Pesquera, G. Herranz, A. Barla, E. Pellegrin, F. Bondino, E. Magnano, F. Sánchez, and J. Fontcuberta, Nat. Commun. **3**, 1189 (2012).

[39] Z. Wang *et al.*, Proc. Natl. Acad. Sci. U.S.A. **111**, 3933 (2014).

[40] E. Stavitski and F. M. F. De Groot, Micron **41**, 687 (2010); F. M. F. de Groot, J. C. Fuggle, B. T. Thole, and G. A. Sawatzky, Phys. Rev. B **41**, 928 (1990); M. Matsubara, T. Uozumi, and A. Kotani, J. Synchrotron Radiat. **8**, 393 (2001).

[41] For the simulations, we used cubic crystal field parameter 10 Dq = 2.0 eV, the charge transfer parameters were $\Delta = 3$ eV, Udd = 4 eV, and Upd = 6 eV, and Lorentzian broadenings were 0.06 eV (for $L_3 - t_{2g}$), 0.22 eV (for $L_3 - e_g$), 0.4 eV (for $L_2 - t_{2g}$), and 0.5 eV (for $L_2 - e_g$). The tetragonal field parameters, Ds and Dt, were varied to fit the experimental data and obtain the energy splittings as $\Delta e_g = 4\,\mathrm{Ds} + 5\,\mathrm{Dt}$ and $\Delta t_{2g} = 3\,\mathrm{Ds} - 5\,\mathrm{Dt}$. The parameter Ds ranged approximately from −10 to 10 meV and Dt from −1 to 1 meV.

[42] S. Caprara, F. Peronaci, and M. Grilli, Phys. Rev. Lett. **109**, 196401 (2012).